IMPERIAL COLLEGE LONDON

Department of Earth Science and Engineering

Centre for Petroleum Studies

Modelling Transport in Heterogeneous Media

By

Dmytro Petrovskyy

A report submitted in partial fulfilment of the requirement for the MSc and/or the DIC

September 2013

DECLARATION OF OWN WORK

I declare that this thesis “Modelling Transport in Heterogeneous Media” is entirely my own work and that where any material could be construed as the work of others, it is fully cited and referenced, and/or with appropriate acknowledgement given.

Signature:.....

Name of student: Dmytro Petrovskyy

Name of supervisor: Prof. Martin Blunt
Dr. Branko Bijeljic

Abstract

The complexity of the pore space of reservoir rocks and related non-Fickian flow behaviour of solute, require new approaches and methodologies for a proper description of transport phenomena. Although modern technologies allow us to scan the pore space geometry to acquire high resolution images and perform direct simulations, we still do not completely understand anomalous transport nature of solute in different types of rock heterogeneities and at multiple scales.

We develop an upscaled advection-dispersion equation (ADE) for large-scale transport which corresponds to a robust pore-scale approach and is in a good agreement with experimental measurements of transport through different rock types (Scheven *et al.*, 2005). We use an ADE with multiple-rate mass transfer (MRMT) as proposed by Haggerty and Gorelick (1995), which subdivides pore space into so-called mobile and immobile regions. This differentiation of the porous medium allows the emergence of different transport behaviour depending on the first order mass transfer rate. We compare and validate our results to the experimental measurements on core samples by Scheven *et al.* (2005) and the pore-scale modelling studies of Bijeljic *et al.* (2013a), and discuss various aspects that cause anomalous transport behaviour. We demonstrate a good agreement with experimental and pore-scale modelling propagators. Furthermore, we relate mass transfer rates to mobile and immobile porosity of the different media, therefore attributing a physical meaning for the mass transfer rates.

Acknowledgement
First of all, I would like to express my gratitude to the best supervisors Dr. Branko Bijeljic and Prof. Martin Blunt. Without your critical assessment of my work as well as accurate guidance throughout the whole duration of my project I will definitely not be able to achieve the same progress I managed to acquire under your supervision. Secondly, I am in debt to my former Ukrainian Ivano-Frankivsk Oil and Gas University for their support with promoting me for the Ukrainian Governmental Scholarship Program.

Above all, I want to thank to my family members, to my always beloved sister Iryna Petrovska, for the mental support and care to my mom Olena Petrovska and of course to my major life supervisor to my father Oleksandr Petrovskyy. Also I want to thank to all of my Ukrainian as well as foreign friends I have found here in London, guys you are the best! Last but not least, I owe my deepest gratitude to Nelya Grymaluk, for her support and all the happiness she brought into my life these days.

Table of Contents

List of Figures

List of Tables

Modelling Transport in Heterogeneous Media

Dmytro Petrovskyy, Martin J. Blunt, Branko Bijeljic, Imperial College London

This paper was prepared for presentation at the Imperial College, London UK, September 2013.

Abstract

The complexity of the pore space of reservoir rocks and related non-Fickian flow behaviour of solute, require new approaches and methodologies for a proper description of transport phenomena. Although modern technologies allow us to scan the pore space geometry to acquire high resolution images and perform direct simulations, we still do not completely understand anomalous transport nature of solute in different types of rock heterogeneities and at multiple scales.

We develop an upscaled advection-dispersion equation (ADE) for large-scale transport which corresponds to a robust pore-scale approach and is in a good agreement with experimental measurements of transport through different rock types (Scheven *et al.*, 2005). We use an ADE with multiple-rate mass transfer (MRMT) as proposed by Haggerty and Gorelick (1995), which subdivides pore space into so-called mobile and immobile regions. This differentiation of the porous medium allows the emergence of different transport behaviour depending on the first order mass transfer rate. We compare and validate our results to the experimental measurements on core samples by Scheven *et al.* (2005) and the pore-scale modelling studies of Bijeljic *et al.* (2013a), and discuss various aspects that cause anomalous transport behaviour. We demonstrate a good agreement with experimental and pore-scale modelling propagators. Furthermore, we relate mass transfer rates to mobile and immobile porosity of the different media, therefore attributing a physical meaning for the mass transfer rates.

Introduction

Pore-scale imaging and modelling has become an important tool to quantify pore scale parameters and predict solute transport. Blunt *et al.* (2013) describe the technology which is nowadays used in the oil and gas industry. Modern X-ray computed tomography (CT) scanners produce high resolution micron-scale three-dimensional images of the pore space. Direct simulation and network modelling are current methodologies to simulate flow and transport through these images. The state of the art technologies and computer hardware allow us to acquire accurate precise images and modelling results for different types of pore-scale heterogeneity.

One of the most descriptive ways to quantify transport of the porous system is to define a propagator – the probability density function of particle displacement as a function of time. Using propagators various attempts have been made to understand the nature of the non-Fickian solute transport at the pore and core scales. Kandhai *et al.* (2002) simulated and measured propagators through the fixed bed of spherical permeable particles. Scheven *et al.* (2005) conducted nuclear magnetic resonance (NMR) measurement of the particles movement through a bead pack, Bentheimer sandstone, and Portland carbonate core samples. These types of rocks represented different degrees of heterogeneity, from an almost homogeneous beadpack to a highly complex carbonate. Characteristic shapes of the propagators showed very high concentration of the stagnant particles in the carbonate sample, less dominant stagnant regions in the case of the sandstone and almost negligible amount of particle retardation in the beadpack. Bijeljic *et al.* (2013) used a direct streamline simulation approach at the pore scale to predict the same experimental propagators and attributed different non-Fickian behaviour to different probability density functions of voxel velocity in the micro-CT images.

In these and other studies (as reviewed in Berkowitz *et al.*, 2006) non-Fickian (anomalous) transport behaviour has been observed in the complex pore space systems from pore to field scale – this complexity and multiple scales require development and establishment of a new theory to fully describe the transport phenomena. Tracer movement governed by a linear increase of the variance of the plume concentration with time is called Fickian transport and is characteristic of homogeneous systems. On the other hand, non-Fickian behaviour is the deviation of the concentration profile with time from the one described by the general ADE with a constant dispersivity, which indicates heterogeneous anomalous behaviour. The latter behaviour cannot be represented by an analytical expression and thus requires different macroscopic approach.

The objective of this project is to find an effective transport equation for use in larger-scale simulation which accurately captures pore-scale heterogeneity. To ensure reliability of an equation we compare propagators for the already known samples, which are the bead pack, Bentheimer sandstone and Portland carbonate. They represent different pore system complexity and produce qualitatively and quantitatively different displacement profiles. The fundamental governing transport equation used in

the study is a multiple-rate transfer model (MRMT) presented by Haggerty and Gorelick (1995).The model defines simultaneous mass transfer between mobile (high velocity) and immobile (low velocity) zones and has advection and diffusion components incorporated. An exchange of a concentration between moveable and stagnant zones is then related proportionally to an exchange rate coefficient for each particular position of the cell in space.

We develop a one-dimensional simulation model as an effective upscaled equivalent to the real three-dimensional system. We constrain it to reproduce precisely the same transport behaviour of a tracer occurred in the three-dimensional space during either the physical experiment or the direct simulations. To validate obtained outcomes we predict propagators (probability density function of particles displacement) and match them to the nuclear magnetic resonance (NMR) experimental results by Scheven *et al.* (2005) and the pore-scale direct simulation results by Bijeljic *et al.* (2013a). We relate mass transfer rates in MRMT model to mobile and immobile porosity of the different media obtained from micro-CT images and show how this relationship varies with heterogeneity.

Methodology and Model Definition

First, we define a general solute transport equation in one dimension to govern the flux in our model. We express original advection-dispersion equation with mass transfer exchange between mobile and immobile phase as

$$\phi_m \frac{\partial C_m}{\partial t} + \phi_{im} \frac{\partial C_{im}}{\partial t} = \phi_m D_L \frac{\partial^2 C_m}{\partial x^2} - q \frac{\partial C_m}{\partial x} \tag{1}$$

where C_m and C_{im} $[mol/m^3]$ stand for concentration in mobile and immobile zones respectively at any given set of (t, x). ϕ_m and ϕ_{im} are mobile and immobile porosities respectively. D_L $[m^2/s]$ is the hydrodynamic dispersion coefficient, q $[m/s]$ is the Darcy velocity defined by flow rate (Q $[m/s^3]$) divided by cross sectional area (A $[m^2]$) perpendicular to the direction of flow. The first order-mass mass transfer model may be defined as

$$\phi_{im} \frac{\partial C_{im}}{\partial t} = \omega \left(C_m - C_{im} \right) \tag{2}$$

where $\omega[s^{-1}]$ – first-order mass transfer rate coefficient. This term represents simultaneous mass transfer between mobile and immobile zones due to the difference in concentrations. Variation of mass transfer rate coefficient is the factor that heavily influences propagators shape with the time evolution, establishing either a stagnant peak or an extensive mobile tail.

To solve numerically the differential equation of multi-rate mass transfer (1), we introduce a finite-difference based one-dimensional simulation model (Figure 1) which consists of uniform grid blocks (Δx is constant) arranged in the direction of flow. Each cell has its own set of mobile $C_m[t, i]$ and immobile $C_{im}[t, i]$ concentrations which evolve with time. Static parameters are the exchange rate $\omega[i]$ and average pore velocity $u[i] = q/(\phi_m[i] + \phi_{im}[i])$.

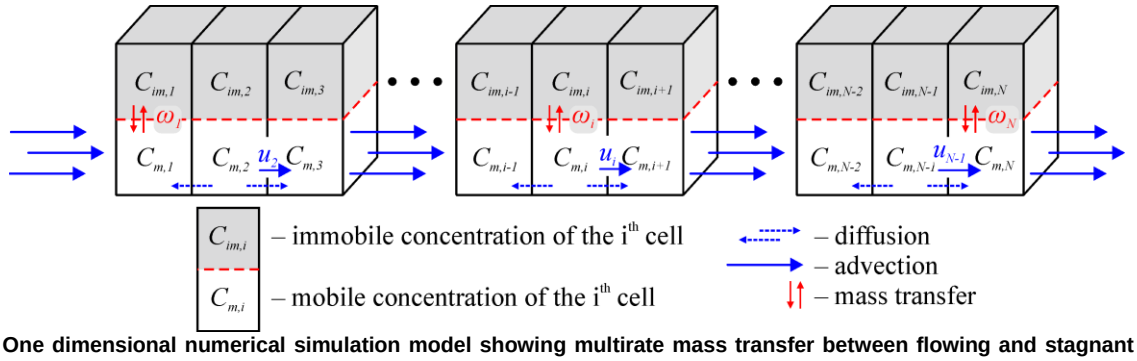

Figure 1 – One dimensional numerical simulation model showing multirate mass transfer between flowing and stagnant regions of the pore space.

Given the fixed values of a grid block size (Δx) and a timestep (Δt), mass change in terms of finite difference approximation is expressed as

$$\begin{aligned}
&\phi_m(x)\,\Delta C_m\left(t+\Delta t, x\right) = && \text{flux}\\
&-\Delta t\,\omega(x)\left(\textbf{if } C_m\left(t,x\right) > C_{im}\left(t,x\right) \textbf{ then } \phi_m(x) \textbf{ else } \phi_{im}(x)\right)\left(C_m\left(t,x\right) - C_{im}\left(t,x\right)\right) && \text{mass transfer}\\
&-\Delta t \Delta x^{-1}\, q\left(\phi_m(x) C_m\left(t,x\right) - \phi_m(x-\Delta x) C_m\left(t,x-\Delta x\right)\right) && \text{advection}\\
&+\Delta t \Delta x^{-2}\, D_L(t) \left(\begin{array}{ll} + \textbf{if } C_m\left(t,x+\Delta x\right) > C_m\left(t,x\right) & \textbf{then } \phi_m(x+\Delta x)\left(C_m\left(t,x+\Delta x\right) - C_m\left(t,x\right)\right) \\ & \textbf{else } -\phi_m(x)\left(C_m\left(t,x\right) - C_m\left(t,x+\Delta x\right)\right) \\ - \textbf{if } C_m\left(t,x\right) > C_m\left(t,x-\Delta x\right) & \textbf{then } \phi_m(x)\left(C_m\left(t,x\right) - C_m\left(t,x-\Delta x\right)\right) \\ & \textbf{else } -\phi_m(x-\Delta x)\left(C_m\left(t,x-\Delta x\right) - C_m\left(t,x\right)\right) \end{array} \right) && \text{dispersion}
\end{aligned} \tag{3}$$

We initialize a model with a given total number of cells (N). We then place initial non-zero concentration (C_{init}) solute in multiple consequent cells ($Nsol$) thus not limiting our model to a single solute placed cell. This is done to generalize the problem and reproduce the NMR experimental conditions in which $\Delta x \times Nsol$ is equal to a side-length of a core sample. We

allow for a particular number of empty cells before the solute placed cells in a direction of flow to capture negative displacement, which is caused by dispersion and diffusion of particles. The total number of the cells is defined to keep solute displacement inside the model and not to exceed boundaries of the model for a total time (T) of a simulation (Figure 2). Eventually, we calculate probability density function of particles displacement for a total simulation time (propagator). However, due to the multi-cell solute initialization approach, related problem of concentration tracking arises. To solve this issue, we introduce decomposition of the total concentration in each cell for either mobile and immobile zones.

For a given number of solute placed cells ($Nsol$) and total number of cells (N) we define a concentration matrix $\mathbf{C}$ for both mobile and immobile regions of the model. $\mathbf{C} = \{C[i, j]\}$ where $i = 1..N$ and $j = 1..Nsol$. Physically, $C[i, j]$ indicates solute concentration in i-th grid block arrived from j-th solute placed cell.

$$\mathbf{C} = \begin{pmatrix} C[1,1] & C[1,2] & C[1,3] & ... & C[1,Nsol] \\ C[2,1] & C[2,2] & C[2,3] & ... & C[2,Nsol] \\ C[3,1] & C[3,2] & C[3,3] & ... & C[3,Nsol] \\ ... & ... & ... & ... & ... \\ C[N,1] & C[N,2] & C[N,3] & ... & C[N,Nsol] \end{pmatrix} \quad (4)$$

Initially mobile concentration ($\mathbf{C_m}$) is at equilibrium with immobile concentration ($\mathbf{C_{im}}$), thus the initialization matrix ($\mathbf{C_{init}}$) may be expressed as

$$\mathbf{C}_{init} = \begin{pmatrix} 0 & 0 & 0 & ... & 0 \\ ... & ... & ... & ... & ... \\ 0 & 0 & 0 & ... & 0 \\ C_{init} & 0 & 0 & ... & 0 \\ 0 & C_{init} & 0 & ... & 0 \\ 0 & 0 & C_{init} & ... & 0 \\ ... & ... & ... & ... & ... \\ 0 & 0 & 0 & ... & C_{init} \\ 0 & 0 & 0 & ... & 0 \\ ... & ... & ... & ... & ... \\ 0 & 0 & 0 & ... & 0 \end{pmatrix} \quad (5)$$

As a result, all the manipulations with solute concentration are governed by linear transformations of mobile and immobile concentration matrices. However, they are not the simplest element-to-element computations, some components of tracer transport approximation require additional data aggregation, thus inducing extra complexity into the numerical algorithms.

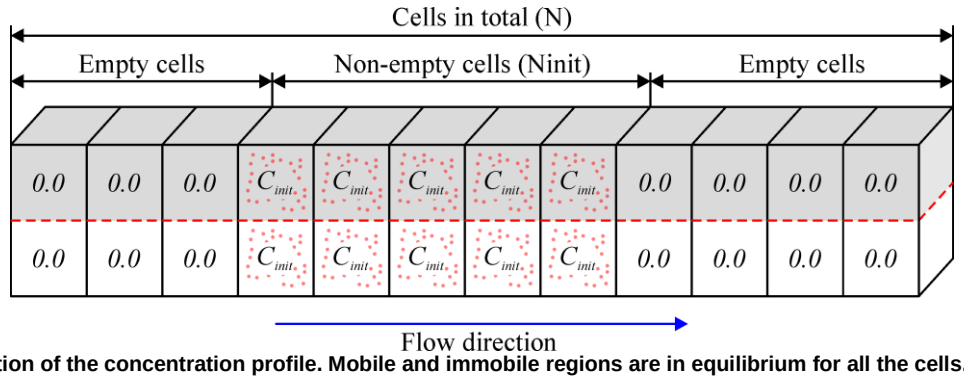

Figure 2 – Initialization of the concentration profile. Mobile and immobile regions are in equilibrium for all the cells.

Finally, to obtain actual displacement profile we calculate a so-called displacement matrix ($\mathbf{C_{disp}}$), which essentially is a transformation of sub-diagonals of the total concentration matrix ($\mathbf{C_m}$+$\mathbf{C_{im}}$). For a given displacement relative number d, where $d = 0$ stands for the base diagonal and $\mathbf{C_{disp}}[0] = \{C_{init}\}$ initially, $d = -1$ for the higher diagonal (negative displacement) and +1 for the lower diagonal (positive displacement), without taking into an account actual matrix dimensions, concentration of particles moved by $d \times \Delta x$ is equal to

$$C_{disp}[d] = \sum_{j=1}^{Nsol} \mathbf{C_{disp}}[d, j] \quad (6)$$

All the highlighted numerical methodology steps are efficiency demanding in terms of computer resources and performance. For example, for a core sample of a side length of 1 mm and Δx = 1 μm, $Nsol$ = 1000 and assume N = 1500, concentration matrix $\mathbf{C}$ is already over 1 million elements. Moreover, to keep convergence of the solution we consider respectively smaller timesteps, for instance Δt = 0.2 μs. Eventually, to simulate 0.1 s of the experiment we run 500 000

simulations over the matrix with over 1 000 000+ elements. Hence, consideration should be given to optimisation of the numerical algorithms to acquire propagator results in a realistic time.

Although the calculations are not perfectly homogeneous, they still can be efficiently parallelized on a multi-core system. For this purpose, computation using a graphics processor unit (GPU) as a state-of-the-art and promising technology of a high performance computing to accelerate engineering and scientific solutions was selected to implement the highlighted methodology. Recently the NVIDIA technology company provided a standardized interface to run programs over various GPUs. Computer unified device architecture (CUDA) is a platform developed by NVIDIA to access parallel computational elements of CUDA compatible GPUs. The CUDA C\C++ programming language (Appendix B) was used as a toolkit to build GPU kernels (functions). As expected, a valuable performance of up to two orders of magnitude boost was acquired (although the GPU actually used was not the most powerful nowadays). Wolfram Mathematica application was used as a front end of data input and GPU output as well as for visualization purposes. Microsoft Visual Studio product was involved in a development of the actual GPU code and intermediate central processor unit (CPU) code to accelerate communication between GPU and Mathematica.

As mentioned before, our goal is to establish the probability distribution function of particles displacement (propagators) for each particular time. In our case, propagators are plotted normalized and non-dimensional $P(\zeta)\times\langle\zeta\rangle_0$ over $\zeta/\langle\zeta\rangle_0$, where ζ is a displacement distance value, mm; $\langle\zeta\rangle_0$ is an average displacement equals to $u_{av}\times T$. $P(\zeta)$ is a probability of a particle to move by ζ mm. Evolution times (T) introduced in the NMR experiments by Scheven *et al.* (2005) are 0.106, 0.2, 0.45, 1.0, 2.0 s. Qualitatively different solute behaviour is observed at early times (0.106 and 0.2 s) compare to the later ones (1.0, 2.0 s). Experimental conditions (Table 1) were taken into an account to establish representative propagators.

We relate mass transfer rate (ω) values to the mobile and immobile porosity and by adjusting the multiplier coefficient acquire the best match. The cell size (Δx) is defined by the CT-scan resolution, time step (Δt) is selected to keep the solution converging depending on the grid block size and dispersion coefficient. The number of cells (*Ninit*) initially containing solute was defined as the ratio of the side length of the core sample (Table 1) divided by Δx. Depending on the cell size we set the total model length (N) large enough to keep the tracer inside the model not leaving boundaries of the model.

Model	u_{av}, mm/s	Side length of the CT-images, mm	Voxel size, μm	Total number of voxels	Peclet number	ϕ_{av}, Scheven *et al.* (2005)	ϕ_{av}, Bijeljic *et al.* (2013)
Bead pack	0.91	0.6	2	300^3	41.4	37%	35.93%
Bentheimer sandstone	1.03	0.9	3	300^3	65.5	23%	21.51%
Portland carbonate	1.26	2.88	9	320^3	187.3	18%	8.62%

Table 1 – Experimental model parameters for each type of heterogeneity.

Porosity Assignment

To establish mobile and immobile porosity profiles for each of the models we extract the data from CT-images obtained by Bijeljic *et al.* (2013a). For a voxelized image of a core sample, porosity is defined as the ratio of the number of pore voxels divided by the total number of voxels. One-dimensional simulation MRMT model requires upscaling of the actual CT-image 2D slices perpendicular to the direction of flow to acquire 1D averaged profile corresponding to MRMT model of the 3D model. The next step is to subdivide porosity into mobile porosity in which advection is dominant and immobile porosity which is characterized by velocities lower than a particular threshold value of velocity. A criterion taken to classify voxels into these categories is the ratio of $t_{adv} = \Delta x/u_{av}$ to $t_{diff} = \Delta x^2/(2D_m)$, which indicates time for a particle to exit the voxel due to advection and diffusion respectively. Given this particular threshold relation and average velocity value of the voxel we may extract different mobile and immobile porosity profiles for each of the samples. We examined three different criteria, which are t_{adv}/t_{diff} = 10, 50, and 100 (profiles are shown in Figure 3–5).

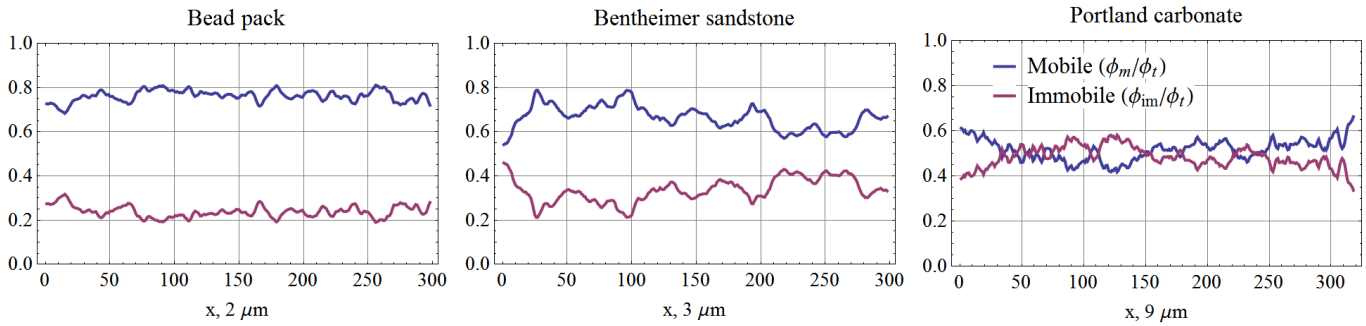

Figure 3 – Porosity profiles extracted from CT-images for each type of heterogeneity for t_{adv}/t_{diff} = 10.

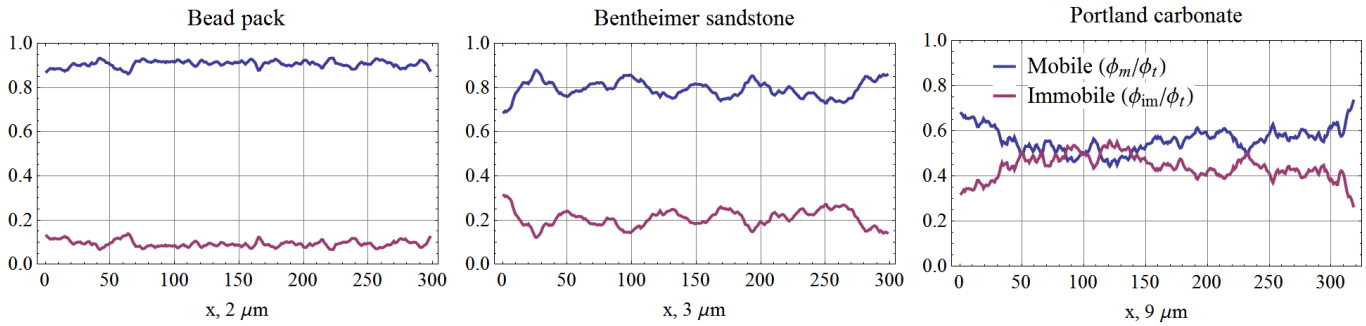

Figure 4 – Porosity profiles extracted from CT-images for each type of heterogeneity for t_{adv}/t_{diff} = 50.

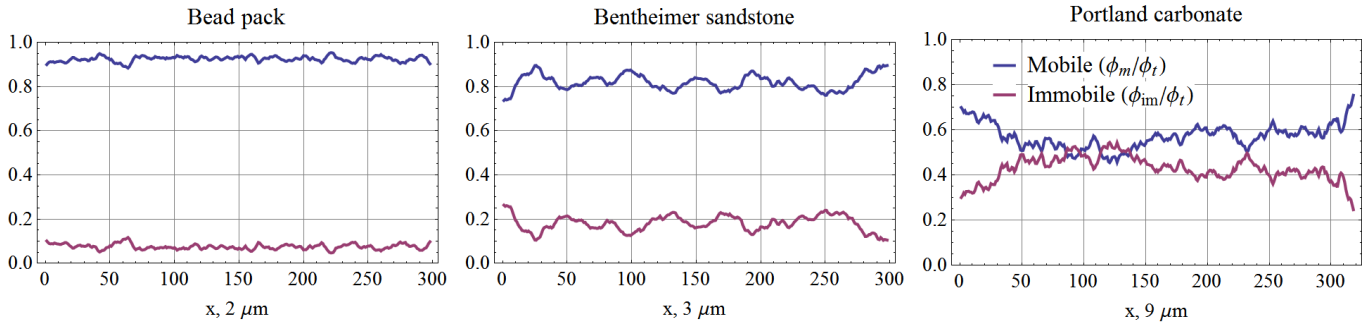

Figure 5 – Porosity profiles extracted from CT-images for each type of heterogeneity for t_{adv}/t_{diff} = 100.

It appears that ratios of t_{adv}/t_{diff} = 50 and 100 result in similar porosity profiles compare to the t_{adv}/t_{diff} = 10, in which mobile porosity is the lowest. Summary of the average mobile porosities with respect to t_{adv}/t_{diff} is presented in Table 2. Qualitatively it is clear that immobile porosity fraction is the smallest in the case of the bead pack and the highest in Portland carbonate. This is true for all the ratios of t_{adv}/t_{diff}. Moreover carbonate porosity profile is highly variable compare to the bead pack and Bentheimer sandstone porosities, there are regions in which immobile porosity is higher than respective mobile porosity.

Model	$\phi_{av}(10)$	$\phi_{av}(50)$	$\phi_{av}(100)$
Bead pack	27.4%	32.6%	33.2%
Bentheimer sandstone	14.2%	17.0%	17.6%
Portland carbonate	4.5%	4.9%	5.0%

Table 2 – Relationship of the average mobile porosity to the t_{adv}/t_{diff} ratio.

Propagators

To capture the actual dispersion of concentration during the simulation we establish dynamic dispersion dependency on time. Bijeljic *et al.* (2011) presents the preasymptotic behaviour of D_L for different types of heterogeneity (a sand pack, sandstone and Portland carbonate) from continuous time random time walks (CTRW) models. As the result, in the model the asymptotic dispersion coefficient is gradually developed and for all the simulation cases ($t \leq 2$ s) in all the types of heterogeneity (Figure 6) we do not reach the asymptotic dispersion value. We examine t_{adv}/t_{diff} = 10 as the most sensible and distinctive profile (Figure 7) compare to t_{adv}/t_{diff} = 50 and 100. We relate mass transfer rate to the squared ratio of immobile to mobile porosity.

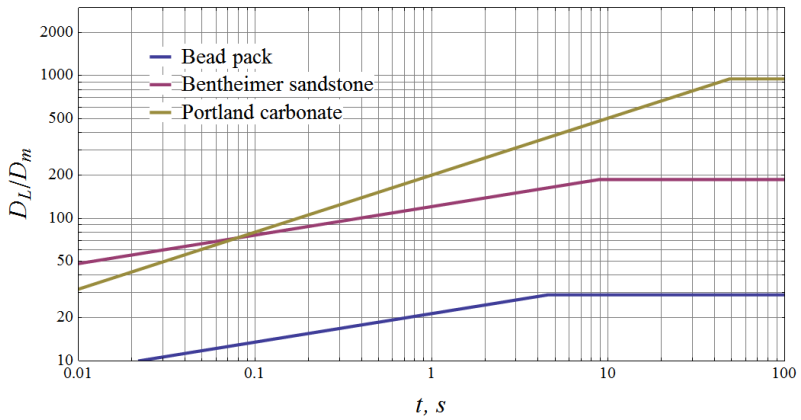

Figure 6 – The preasymptotic and asymptotic behaviour of dispersion coefficient for different types of heterogeneity.

As expected, the least heterogeneous pore space of the bead pack produce the least anomalous behaviour. However, at early times, the actual propagator profile is not symmetrical, which indicates non-Fickian transport response, even in the case of the almost homogenous porous media. At mid-time (0.45 s) of the simulation the shape is normalized and the mean value of displacement is equal to 1 representing both immobile and mobile concentration simultaneous movement, also the plume profile is becoming Gaussian representing Fickian behaviour. As time evolves, Gaussian shape remains and propagator only gets narrowed. Due to a highly homogeneous pore structure and small influence of the dispersion on the tracer transport, propagators (Figure 8) are in a good agreement with those presented by Scheven *et al.* (2005) and by Bijeljic *et al.* (2013a) for all the five time snapshots. The main problem related to this type of the heterogeneity is a slight overestimation at early times and a gradual underestimation at late times compared to the observed ones from NMR experiment and pore-scale modelling.

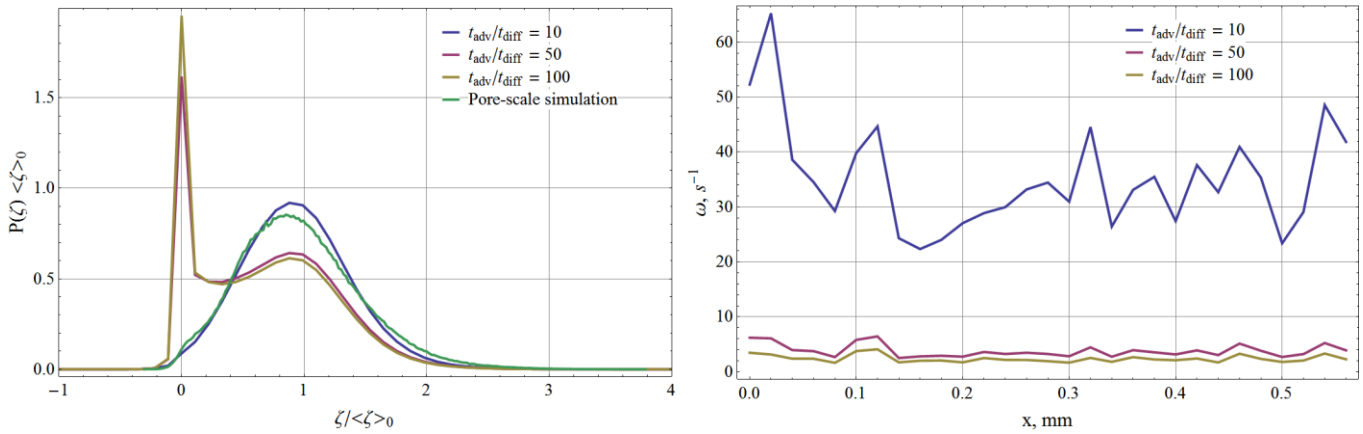

Figure 7 – The bead pack propagator dependency on t_{adv}/t_{diff} as obtained from the actual mobile and immobile porosity distribution. t_{adv}/t_{diff} take values of 10, 50, 100. ω = 350 $(\phi_{im}/\phi_m)^2$, T = 0.2 s, Δx = 20 μm (10 voxels).

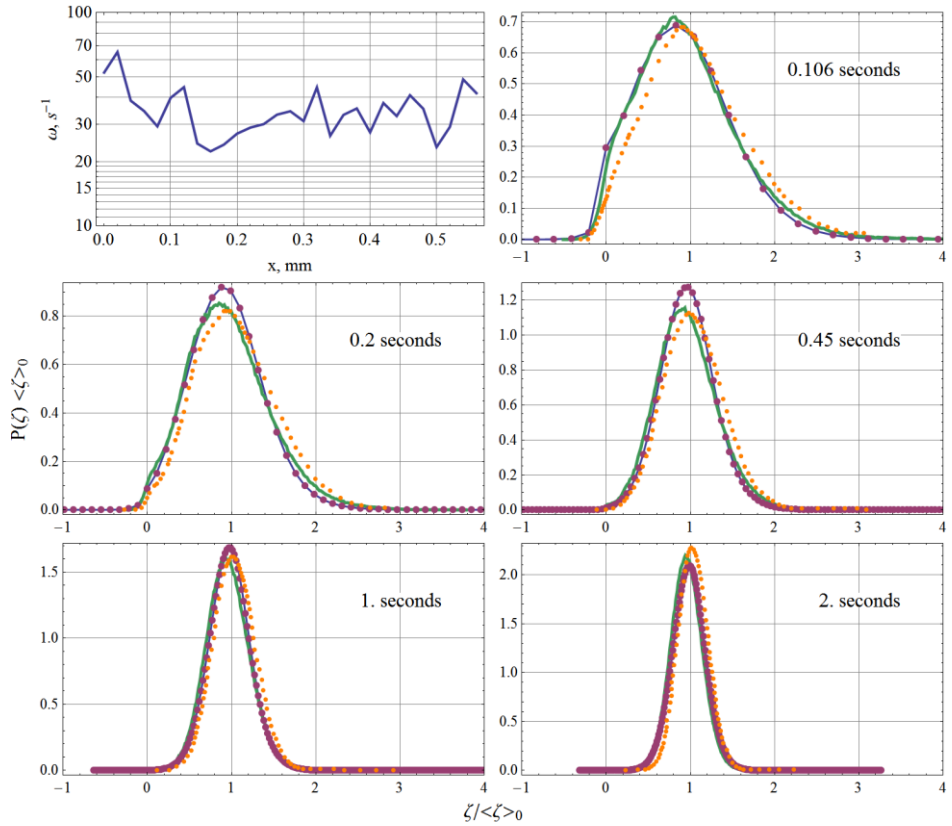

Figure 8 – The bead pack propagators and the matching mass transfer rate profile, Δx = 20 μm (10 voxels), ω = 350 $(\phi_{im}/\phi_m)^2$. Orange dotted – NMR experiments by Scheven *et al.* (2005). Green solid – streamline simulation by Bijeljic *et al.* (2013a). Blue solid and purple dotted – multi-rate transfer model.

In the case of Bentheimer sandstone, at early times we observe a clear stagnant peak which spreads out due to influence of particle diffusion and dispersion. As time progresses, the immobile peak fades out and a second mobile hump gradually develops. Eventually, after 2 s of the experiment, the moving region becomes dominant and governs the overall flow. As the result, even low level of heterogeneity may establish mobile and immobile regions in a rock and thus developing two different

zones of displacement. Propagators obtained by MRMT model for Bentheimer sandstone have dominant immobile peaks with a sharper decrease at the first and the second time studied (0.106 and 0.2 s) compared to the gradual decrease observed in the NMR experiment and pore-scale simulation. This could be due to the fact that between MRMT cells a constant displacement is recorded in MRMT model, whereas in the NMR experiment and pore-scale simulation (Figure 9) the exact positions in the cells are known and therefore displacement is calculated more accurately. As for the mid-time and late time, good agreement is observed. Upscaling of the grid was conducted from 3 μm (CT-image resolution) up to 30 μm (Figure 10).

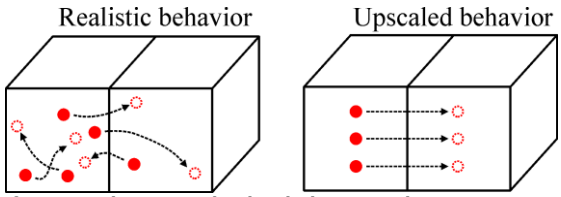

Figure 9 – Particles motion in the case of NMR and pore-scale simulation experiments compare to the implemented upscaled model.

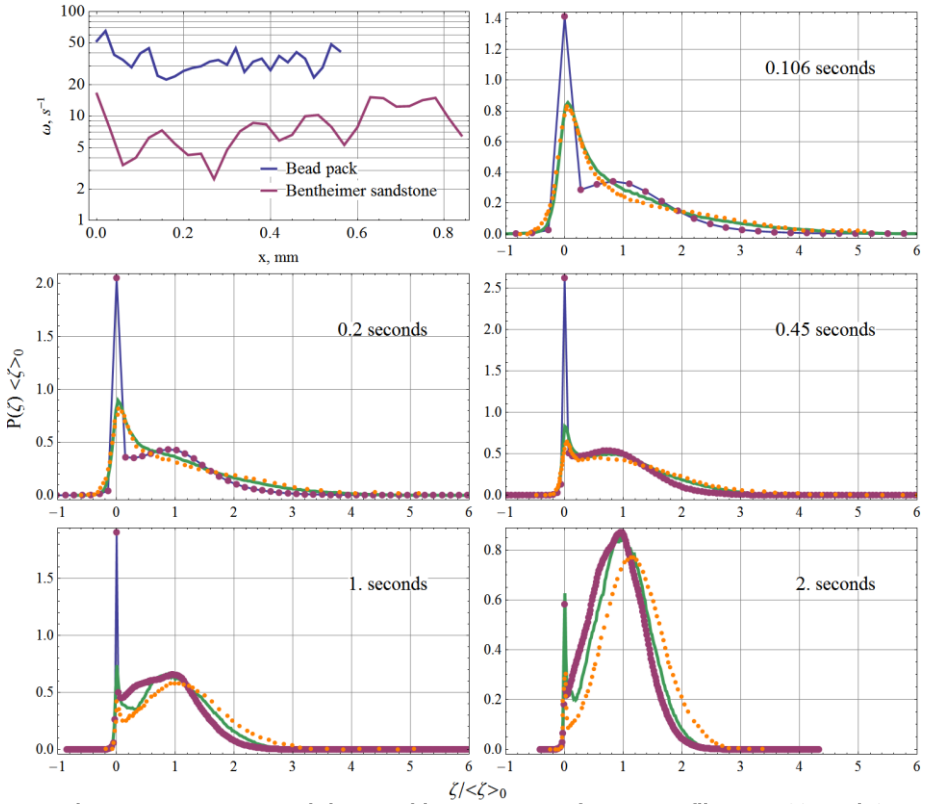

Figure 10 – Bentheimer sandstone propagators and the matching mass transfer rate profile, Δx = 30 μm (10 voxels), ω = 30 $(\phi_{im}/\phi_m)^2$. Orange dotted – NMR experiments by Scheven *et al*. (2005). Green solid – streamline simulation by Bijeljic *et al*. (2013a). Blue solid and purple dotted – multi-rate transfer model.

On the other hand, the most heterogeneous and complex Portland carbonate has a persistent and dominant immobile peak for the whole time of the experiment (up to 2 s). Only at late time (more than 1 s) establishment of a mobile hump occurs, although it is very wide due to high dispersion in this rock (Figure 11). Early breakthrough for carbonates is not an unusual behaviour. Various types of carbonates heterogeneity have been studied specifically by Bijeljic *et al.* (2013b). This type of the pore complexity is the least explored and that is why it requires additional research and analysis. The most heterogeneous carbonate propagators are the most difficult to reproduce due to the extremely anomalous behaviour and high dependency on the dispersion of the particles. As for the development of Fickian behaviour in Portland carbonate, we may observe mobile zone dominating after 5 s and final smoothed Gaussian shape with almost no immobile impact after 10 s (Figure 12), although we do not take into an account micro-porosity impact.

Results of the sensitivity analysis concluded that inherent discontinuity of the displacements between the cells in multi-rate mass transfer model results in the sharp (rather than gradual decrease as in the case of the NMR experiment and pore-scale simulation) in the propagator after the immobile peak in the case of both Bentheimer sandstone and Portland carbonate. The second mobile hump is mainly governed by a definition of the correct exchange rate profile and thus relatively easy to match. Early time behaviour agreement of the propagators was not reached due to already mentioned discontinuity issue. Finally, the presence of the multiple models which give the same response in terms of the propagators may introduce non-uniqueness in the solution. To reduce this problem, we have to include additional petrophysical data that will constrain our model and limit the number of solutions.

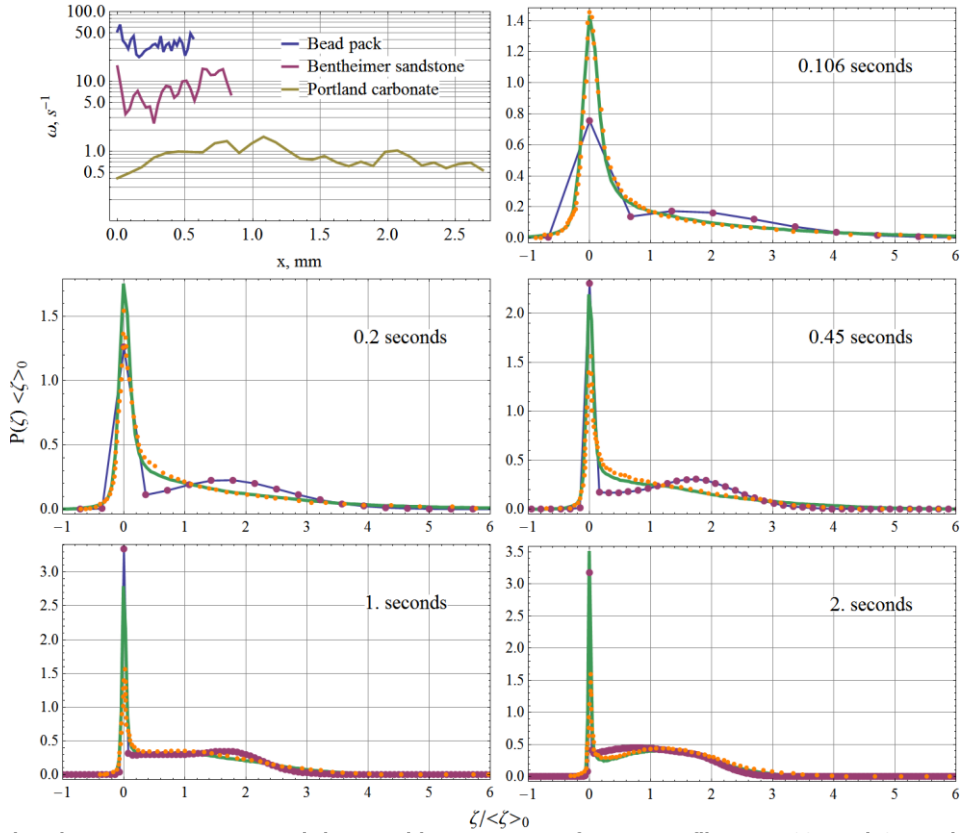

Figure 11 – Portland carbonate propagators and the matching mass transfer rate profile, Δx = 90 μm (10 voxels), ω = 0.9 $(\phi_{im}/\phi_m)^2$. Orange dotted – NMR experiments by Scheven *et al*. (2005). Green solid – streamline simulation by Bijeljic *et al*. (2013a). Blue solid and purple dotted – multi-rate transfer model.

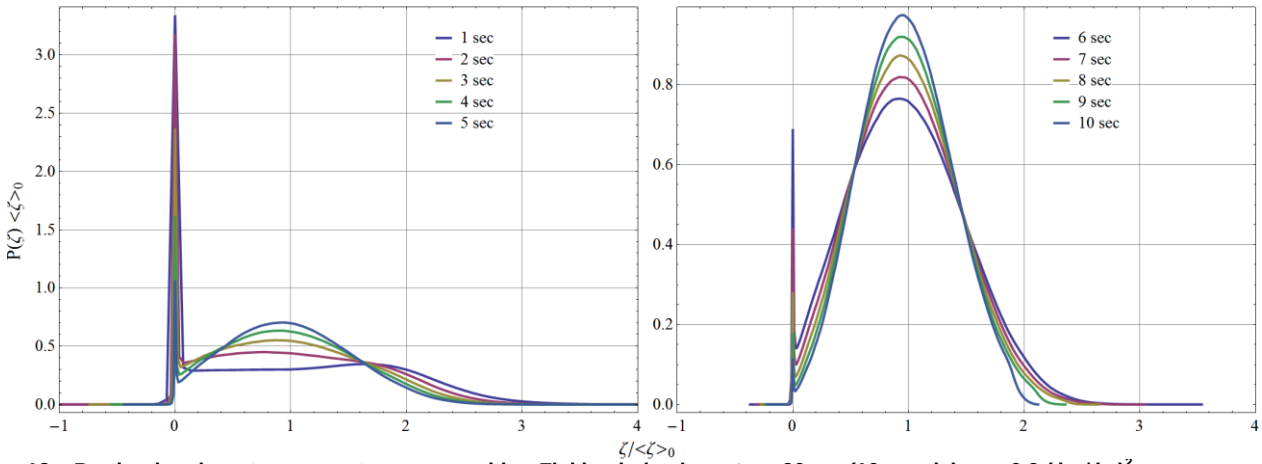

Figure 12 – Portland carbonate propagators approaching Fickian behaviour, Δx = 90 μm (10 voxels), ω = 0.9 $(\phi_{im}/\phi_m)^2$.

Discussion

Each type of heterogeneity define fundamentally different probability density functions for a displacement of solute particles. Conventional reservoir rocks like sandstones and carbonates are influenced by stagnant regions of slower velocities thus developing immobile peaks in propagators at early times of transport, although with further time evolution mobile particles become dominant in the case of the sandstone. However, the most complex in terms of heterogeneity are carbonate rocks in which immobile concentration is dominant and persistent for much longer time compare to the one in the sandstones. Complex dual and multi-porosity systems define this anomalous behaviour and cause particles retardation, that establish immobile peak and respectively prolonged mobile tail characterized by an early breakthrough of the solute.

Different approaches of the particles displacement measurements such as NMR by Scheven *et al.* (2005), direct streamline simulation by Bijeljic *et al.* (2013a) as well as multi rate mass transfer model demonstrated non-Fickian behaviour of the real core samples. MRMT model showed a good agreement between simulated propagators and the ones obtained by NMR experiment and direct pore scale simulation, especially at later times. Further improvement of the model may solve a mismatch with a discontinuity of an immobile region, which is developed by the multi rate model with current definition. We introduced

possible upscaling examples to reproduce the same response with coarser grid. As a first approximation, we related mass transfer rate to the squared ration of immobile to mobile porosity. Exchange rates are of a different order of magnitude of each type of heterogeneity – the highest for the bead pack and the lowest for Portland Carbonate. Results were consistent when the grid scale was sufficiently fine to build a smooth propagator.

Conclusions

In this paper we present a methodology to link a macroscopic description of transport in pore space to the experimental results and pore-scale simulation. A multi-rate mass transfer model has been developed as a solution for a description of the non-Fickian behaviour of solute transport. We used a finite difference numerical approach to simulate flow in different heterogeneous systems. We compared NMR experimental results by Scheven *et al.* (2005) and pore-scale direct simulation by Bijeljic *et al.* (2013a) to the propagators acquired by solution of the multi-rate mass transfer model introduced by Haggerty and Gorelick (1995). Qualitative features related to mobile and immobile regions that result in the different probability distributions functions of the displacement for the bead pack, Bentheimer sandstone and Portland carbonate obtained by MRMT model are in a good agreement with NMR experiments by Scheven *et al.* (2005) and direct streamline simulation by Bijeljic *et al.* (2013). We presented possible relationship between mobile and immobile porosities with mass transfer rate. This study is of an importance for a prediction of transport in highly heterogeneous and complex carbonate reservoirs. MRMT model introduce methodology to capture micro-scale heterogeneity in larger-scale simulations and may be used to simulate field-scale solute displacement.

Nomenclature

C_m = concentration in the mobile zone, mol/m^3
C_{im} = concentration in the immobile zone, mol/m^3
Q = flow rate, m^3/s
A = cross sectional area, m^2
q = Darcy velocity, m/s
D_L = dispersion coefficient, m^2/s
D_m = diffusion coefficient, m^2/s
ω = first-order mass transfer rate coefficient, s^{-1}
L = characteristic length, m
u = average velocity, m/s
Δx = grid block size, m
Δt = timestep, s
N = total number of the cells in the model
$Ninit$ = number of solute placed cells in the model
T = simulation time, s
$\mathbf{C}$ = concentration matrix
ϕ = porosity
ϕ_m = mobile porosity
ϕ_{im} = immobile porosity
ζ = displacement, m
$<\zeta>_0$ = average displacement, m
$P(\zeta)$ = probability of the particle displacement

References

Berkowitz B., Cortis A., Dentz M., Scher H., 2006: "Modelling non-Fickian transport in geological formations as a continuous time random walk", Reviews of Geophysics, Vol. 44, No. 2.

Bijeljic B., Mostaghimi P., Blunt M.J., 2011: "Signature of non-Fickian solute transport in complex heterogeneous porous media", Physical Review Letters, Vol. 107, N. 204502.

Bijeljic B., Mostaghimi P., Blunt M.J., 2013b: "Insights into non-Fickian solute transport in carbonates", Water Resources Research, Vol. 49, No. 5, p. 2714–2728.

Bijeljic B., Raeini A., Mostaghimi P., Blunt M.J., 2013a: "Predictions of non-Fickian solute transport in different classes of porous media using direct simulation on pore-scale images", Physical Review E, Vol. 87, No. 1, p. 013011-1–013011-9.

Blunt M.J., Bijeljic B., Dong H., Gharbi O., Iglauer S., Mostaghimi P., Paluszny A., Pentland C., 2013: "Pore-scale imaging and modelling", Advances in Water Resources, Vol. 51, p. 197-216.

Haggerty R., Gorelick S.M., 1995: "Multiple-rate mass transfer for modelling diffusion and surface reactions in media with pore-scale heterogeneity", Water Resources Research, Vol. 31, No. 10, p. 2383–2400.

Kandhai D., Hlushkou D., Hoekstra A.G., Sloot P.M.A., Van As H., Tallarek U., 2002: "Influence of stagnant zones on transient and asymptotic dispersion in macroscopically homogeneous porous media", Physical Review Letters, Vol. 88, No. 23, p. 234501-1–234501-4.

Scheven U., Verganelakis D., Harris R., Johns M., Gladden L., 2005: "Quantitative nuclear magnetic resonance measurements of preasymptotic dispersion in flow through porous media", Physics of Fluids, Vol. 17, No. 11, 117107-1–117107-7.

Appendix A – Literature Review

Year	Source	Title	Authors	Contribution
2013b	Water Resources Research, Vol. 49, p. 2714–2728	Insights into non-Fickian solute transport in carbonates	Bijeljic B., Mostaghimi P., Blunt M.J.	Propagators have been acquired for six different carbonate rock samples with relation to different Pe numbers
2013a	Physical Review E, Vol. 87, No. 1	Predictions of non-Fickian solute transport in different classes of porous media using direct simulation on pore-scale images	Bijeljic B., Raeini A., Mostaghimi P., Blunt M.J.	Simulated solute transport through millimetre-sized voxelized 3D images of a beadpack, sandstone and carbonate.
2013	Advances in Water Resources, Vol. 51, p. 197-216	Pore-scale imaging and modelling	Blunt M.J., Bijeljic B., Dong H., Gharbi O., Iglauer S., Mostaghimi P., Paluszny A., Pentland C.	Imaging of pore-space of beadpack, sandstone and carbonate with nanometre scale. Simulation of single and multi-phase flow through these images.
2012	SPE Vol. 17, No. 4, ID 135261-PA	Simulation of flow and dispersion on pore-space images	Mostaghimi P., Bijeljic B., Blunt M.J.	Study of solute transport using direct methods. Streamline and random-walk algorithms are used.
2011	Physical Review Letters, Vol. 107, N. 20	Signature of non-Fickian solute transport in complex heterogeneous porous media	Bijeljic B., Mostaghimi P., Blunt M.J.	Prediction of the concentration profile as a function of Peclet number and time.
2009	Advances in Water Resources, Vol. 32, No. 5	Perspective on theories of non-Fickian transport in heterogeneous media	Neuman S., Tartakovsky D.	Comparison of the four different methods to describe advection and dispersion of passive tracers in porous media of anomalous transport.
2006	Reviews of Geophysics, Vol. 44, No. 2	Modelling non-Fickian transport in geological formations as a continuous time random walk	Berkowitz B., Cortis A., Dentz M., H. Scher	Development of the mathematical continuous time random walk (CTRW) transport methodology.
2005	Physics of Fluids, Vol. 17, No. 11	Quantitative nuclear magnetic resonance measurements of preasymptotic dispersion in flow through porous media	U. Scheven, D. Verganelakis, R. Harris, M. Johns, L. Gladden	Measurements of the preasymptotic Stokes flow through the beadpack, sandstone and carbonate using NMR.
2000	Water Resources Research, Vol. 36, No. 12	On the late-time behaviour of tracer test breakthrough curves	Haggerty R., McKenna S.A., Meigs L.C.	Study of the late-time behaviour of the tracer breakthrough curves (BTC) in multi-porosity systems.
1995	Water Resources Research, Vol. 31, No. 10	Multiple-rate mass transfer for modelling diffusion and surface reactions in media with pore-scale heterogeneity	Haggerty R., Gorelick S.M.	Developed multi-rate model to describe mass transfer between immobile and mobile zones.
1995	Water Resources Research, Vol. 31, No. 6	On characterization of anomalous dispersion in porous and fractured media	Berkowitz B., H. Scher	Study of the anomalous dispersion as the time dependent function using continuous time random walk (CTRW).

Water Resources Research, Vol. 49, p. 2714–2728 (2013b)
Insights into non-Fickian solute transport in carbonates

Authors: Bijeljic B., Mostaghimi P., Blunt M.J.

Contribution to the understanding of modelling transport in heterogeneous media:
Propagators (probability distribution function of particles displacement) have been acquired for six different carbonate rock samples with relation to different Pe numbers (impact of advection and diffusion). Particles retardation as the result of velocity distribution was quantitatively analysed.

Objective of the paper:
Study of non-Fickian transport of plume to represent different nature of anomalous behaviour in carbonates.

Methodology used:
Simulation of solute transport thorough 3D X-ray images of six different carbonate rocks, which represent different types of pore structure complexity. Stokes solver is used to compute flow field. Advection is computed by streamline approach, random time walk method is used for diffusion.

Conclusion reached:
Stagnant peak with a prolonged mobile tail of propagators in carbonates is characteristic for this type of pore complexity. The anomalous response is governed by a wide distribution of velocities and relative influence of diffusion.

Comments:
For the first time, such paper incorporates analysis of the six samples of carbonates altogether. Four of them are Indiana, Estaillades, Ketton, and Mount Gambier limestones and two other are from Middle East aquifer denoted Middle East carbonate 1 (ME1) and Middle East carbonate 2 (ME2). Two types of transport behaviour in carbonates are observed.

Physical Review Letters, Vol. 107, N. 20 (2011)
Signature of non-Fickian solute transport in complex heterogeneous porous media

Authors: Bijeljic B., Mostaghimi P., Blunt M.J.

Contribution to the understanding of modelling transport in heterogeneous media:
Establishment of preasymptotic and asymptotic behaviour of dispersion coefficient for different types of heterogeneity depending on Peclet number and evolution time.

Objective of the paper:
Simulate transport of a solute though three-dimensional images of a sand pack, Berea sandstone, and Portland limestone. Predict the propagators and the dispersion coefficient as a function of Peclet number and time.

Methodology used:
Simulation of solute transport through 3D CT-images of different rock samples. Multirate mass transfer models and continuous random time walk (CRTW) were used to describe non-Fickian transport.

Conclusion reached:
Carbonates are described by a high non-Fickian behaviour with a very high retarded solute concentration, and a non-linear scaling of dispersion coefficient depending on Peclet number.

Physical Review E, Vol. 87, No. 1 (2013a)
Predictions of non-Fickian solute transport in different classes of porous media using direct simulation on pore-scale images

Authors: Bijeljic B., Raeini A., Mostaghimi P., Blunt M.J.

Contribution to the understanding of modelling transport in heterogeneous media:
Very good agreement between the propagators presented in this work and the ones obtained by Scheven et al. (2005) using nuclear magnetic resonance (NMR) experiments is acquired thus proving the robust pore-scale modelling approach.

Objective of the paper:
Predict transport though 3D voxelized CT-images of a bead pack, Bentheimer sandstone, and Portland carbonate representing different heterogeneity. Compute propagators depending on the velocity distribution and obtain decent match between NMR experimental results of Scheven et al. (2005) and conducted pore-scale simulations.

Methodology used:
Simulation of solute transport thorough 3D CT-images of the bead pack, Bentheimer sandstone, and Portland carbonate, which represent different types of pore structure complexity. Stokes solver is used to compute flow field. Advection is computed by streamline approach, random time walk method is used for diffusion.

Conclusion reached:
Homogeneous pore space systems with narrow velocity distribution evolve to the Fickian behaviour quite rapidly. On the other hand, realistic heterogeneity of Bentheimer sandstone shows stagnant peak at early times, although with time progression mobile region eventually dominates. Finally, for Portland carbonate we observe persistent particles retardation during the whole experiment time indicating highly anomalous behaviour.

Advances in Water Resources, Vol. 51, p. 197-216 (2013)
Pore-scale imaging and modelling

Authors: Blunt M.J., Bijeljic B., Dong H., Gharbi O., Iglauer S., Mostaghimi P., Paluszny A., Pentland C.

Contribution to the understanding of modelling transport in heterogeneous media:
Description of pore-scale modelling and imaging as a digital core analysis in general. Discussion of different imaging techniques and modelling methods as well as dispersion impact on solute transport.

Objective of the paper:
Conclude the limitations and challenges of pore-scale imaging and modelling. Imaging and simulating transport in pore spaces of different orders of magnitude up to field scale.

Methodology used:
X-ray tomography, micro CT-scanners, focused ion beams, statistical reconstruction are for pore space imaging. Direct modelling methods and network modelling are the ones used to compute solute transport.

Conclusion reached:
Pore-scale imaging and modelling may be used for analysis of contaminant transport, carbon dioxide storage, and improved oil recovery. Although the problem to of field-scale simulation is still not solved and thus requires additional study.

Physics of Fluids, Vol. 17, No. 11 (2005)
Quantitative nuclear magnetic resonance measurements of preasymptotic dispersion in flow through porous media

Authors: U. Scheven, D. Verganelakis, R. Harris, M. Johns, L. Gladden

Contribution to the understanding of modelling transport in heterogeneous media:
Probability displacement profiles as a function of displacement (propagators) were acquire for a bead pack, Bentheimer sandstone, and Portland carbonate cores at 0.106, 0.2, 0.45, 1, 2s evolution times.

Objective of the paper:
Understand anomalous behaviour of different types of pore complexity.

Methodology used:
Nuclear magnetic resonance measurement were conducted to observe molecular displacement of particles in preasymptotic Stokes flow though a bead pack, Bentheimer sandstone, and Portland carbonate rock samples.

Conclusion reached:
The displacement profile of solute transport is govern by microscopic heterogeneity. Highly porous and good sorted bead pack represent almost homogeneous, compare to more realistic and heterogeneous sandstone and carbonate samples.

Comments:
Beads diameter is from 80 to 120 μm. Peclet and Reynolds numbers are from 20 to 80 and less than 0.1 respectively.

Water Resources Research, Vol. 31, No. 10 (1995)
Multiple-rate mass transfer for modelling diffusion and surface reactions in media with pore-scale heterogeneity

Authors: Haggerty R., Gorelick S.M.

Contribution to the understanding of modelling transport in heterogeneous media:
Multi-rate mass transfer model has been developed to describe simultaneous exchange between mobile and immobile regions of porous media. Other specific cases such as spherical, cylindrical, and layered diffusion models have been presented as well.

Objective of the paper:
The goal of the paper is to develop a general model to represent an upscaled anomalous solute transport subdividing media into so called mobile and immobile zones.

Conclusion reached:
Various first-order mass transfer models are essentially the same to describe transport phenomena.

Appendix B – Computer Program

Essential parts of the program implemented using CUDA technology presented here.

Simulation CUDA kernel definition

`immobileC` – immobile concentration matrix,
`mobileC` – mobile concentration matrix,
`immobileTotalC`– total immobile concentration vector,
`mobileTotalC` – total mobile concentration matrix,
`dt` – timestep,
`W` – mass transfer rate vector,
`advTerm` – precalculated advection term,
`dispTerm` – precalculated dispersion term,
`diffTerm` – precalculated diffusion term,
`immobilePhi` – immobile porosity vector,
`mobilePhi` – mobile porosity vector,
`resultingImmobileC` – output immobile concentration matrix,
`resultingMobileC` – output mobile concentration matrix.

```
__global__ void RunArbitrarySimulation(
        double *immobileC, double *mobileC,
        double *immobileTotalC, double *mobileTotalC,
        double dt, double *W, double advTerm, double dispTerm, double diffTerm,
        double* immobilePhi, double* mobilePhi,
        double *resultingImmobileC, double *resultingMobileC)
{
        __shared__ double Cm[TileSize];
        __shared__ double Cim[TileSize];
        __shared__ double Cm_total[TileSize];
        __shared__ double Cim_total[TileSize];
        __shared__ double mAdv[TileSize - 1];
        __shared__ double mDisp[TileSize - 1];
        __shared__ double imDiff[TileSize - 1];

        double exchange;

        int tile_i = threadIdx.x;
        int i = threadIdx.x + blockIdx.x*(blockDim.x - 2);

        double mobilePhi_i = mobilePhi[i];
        double immobilePhi_i = immobilePhi[i];

        Cm[tile_i] = mobileC[Idx(i, blockIdx.y, gridDim.y)];
        Cim[tile_i] = immobileC[Idx(i, blockIdx.y, gridDim.y)];

        Cm_total[tile_i] = mobileTotalC[i];
        Cim_total[tile_i] = immobileTotalC[i];

        __syncthreads();

        if (tile_i < TileSize - 1) {
                exchange = dt*W[i]*(Cm[tile_i] > Cim[tile_i] ? mobilePhi_i : immobilePhi_i)*(Cm[tile_i] -
Cim[tile_i]);

                mAdv[tile_i] = advTerm*Cm[tile_i];

                mDisp[tile_i] = dispTerm*(
                        Cm_total[tile_i + 1] > Cm_total[tile_i]
                        ? mobilePhi[i + 1]*Cm[tile_i + 1]*(1 - Cm_total[tile_i]/Cm_total[tile_i + 1])
                        : mobilePhi_i*-Cm[tile_i]*(1 - Cm_total[tile_i + 1]/Cm_total[tile_i]));

                imDiff[tile_i] = diffTerm*(
                        Cim_total[tile_i + 1] > Cim_total[tile_i]
                        ? immobilePhi[i + 1]*Cim[tile_i + 1]*(1 - Cim_total[tile_i]/Cim_total[tile_i + 1])
                        : immobilePhi_i*-Cim[tile_i]*(1 - Cim_total[tile_i + 1]/Cim_total[tile_i]));
        }

        __syncthreads();
```

```
        if (0 < tile_i && tile_i < TileSize - 1) {
                resultingImmobileC[Idx(i, blockIdx.y, gridDim.y)] =
                        Cim[tile_i] + (exchange + imDiff[tile_i] - imDiff[tile_i - 1])/immobilePhi_i;
                resultingMobileC[Idx(i, blockIdx.y, gridDim.y)] =
                        Cm[tile_i] + (-exchange + mAdv[tile_i] - mAdv[tile_i - 1]
                        + mDisp[tile_i] - mDisp[tile_i - 1])/mobilePhi_i;
        }
}
```

Displacement calculation CUDA kernel definition

`immobileC` – immobile concentration matrix,
`mobileC` – mobile concentration matrix,
`modelSize` – model size,
`injCells` – solute placed cells,
`start` – initial solute placed cell,
`dx` – cell size,
`avgDisp` – average displacement,
`result` – resulting propagator matrix.

```
__global__ void ConcentrationToDisplacement(
        double* immobileC, double* mobileC,
        int modelSize, int injCells, int start, double dx, double avgDisp, double* result) {
        int num = blockDim.x*blockIdx.x + threadIdx.x;
        int i;
        double sum = 0;
        int total = modelSize + injCells - 1;

        if (num < total) {
                if (num < injCells) {
                        i = (injCells - 1) - num;
                        for (int j = 0; j < Min(injCells - i, modelSize); j++)
                                sum += mobileC[(Idx(j, i+j, injCells))] + immobileC[(Idx(j, i+j, injCells))];
                }
                else {
                        i = num - (injCells - 1);
                        for (int j = 0; j < Min(modelSize - i, injCells); j++)
                                sum += mobileC[(Idx(i+j, j, injCells))] + immobileC[(Idx(i+j, j, injCells))];
                }

                result[Idx(num, 0, 2)] = (num + 1 - start - injCells)*dx/avgDisp;
          result[Idx(num, 1, 2)] = sum;
        }
}
```

Mathematica to CUDA interface function

`libData` – object for the Mathematica data manipulation,
`Argc` – number of arguments,
`Args` – actual arguments,
`Res` – result (propagator).

```
EXTERN_C DLLEXPORT int ComputeArbitraryPropagator(WolframLibraryData libData, mint Argc, MArgument *Args, MArgument
Res) {
        mreal* initCm = libData->MTensor_getRealData(MArgument_getMTensor(Args[0]));
        mreal* initCim = libData->MTensor_getRealData(MArgument_getMTensor(Args[1]));
        mint modelSize = MArgument_getInteger(Args[2]);
        mint injCells = MArgument_getInteger(Args[3]);
        mint start = MArgument_getInteger(Args[4]);
        mreal* W = libData->MTensor_getRealData(MArgument_getMTensor(Args[5]));
        mreal q = MArgument_getReal(Args[6]);
        mreal* immobilePhi = libData->MTensor_getRealData(MArgument_getMTensor(Args[7]));
        mreal* mobilePhi = libData->MTensor_getRealData(MArgument_getMTensor(Args[8]));

        mreal dt = MArgument_getReal(Args[9]);
        mreal dx = MArgument_getReal(Args[10]);
        mreal* dispCoef = libData->MTensor_getRealData(MArgument_getMTensor(Args[11]));
        mreal diffCoef = MArgument_getReal(Args[12]);
        mint simulations = MArgument_getInteger(Args[13]);
        mreal avgDisp = MArgument_getReal(Args[14]);
```

```
mint dispLength = (modelSize - 2) + injCells - 1;

double advTerm = -dt/dx*q;
double dispTerm;
double diffTerm = dt/(dx*dx)*diffCoef;
// GPU
double* temp;

double* dev_mobileC;
double* dev_immobileC;
double* dev_targetMobileC;
double* dev_targetImmobileC;

double* dev_mobilePhi;
double* dev_immobilePhi;
double* dev_W;
double* dev_disp;
double* dev_totalMobileC;
double* dev_totalImmobileC;

double* disp = (double*) malloc(2*dispLength*sizeof(double));

cudaMalloc((void**) &dev_mobileC, modelSize * injCells * sizeof(double));
cudaMalloc((void**) &dev_immobileC, modelSize * injCells * sizeof(double));
cudaMalloc((void**) &dev_targetMobileC, modelSize * injCells * sizeof(double));
cudaMalloc((void**) &dev_targetImmobileC, modelSize * injCells * sizeof(double));

cudaMalloc((void**) &dev_W, modelSize * sizeof(double));
cudaMalloc((void**) &dev_immobilePhi, modelSize * sizeof(double));
cudaMalloc((void**) &dev_mobilePhi, modelSize * sizeof(double));
cudaMalloc((void**) &dev_totalMobileC, modelSize * sizeof(double));
cudaMalloc((void**) &dev_totalImmobileC, modelSize * sizeof(double));
cudaMalloc((void**) &dev_disp, 2 * dispLength * sizeof(double));

cudaMemcpy(dev_mobileC, initCm, modelSize * injCells * sizeof(double), cudaMemcpyHostToDevice);
cudaMemcpy(dev_targetMobileC, initCm, modelSize * injCells * sizeof(double), cudaMemcpyHostToDevice);

cudaMemcpy(dev_immobileC, initCim, modelSize * injCells * sizeof(double), cudaMemcpyHostToDevice);
cudaMemcpy(dev_targetImmobileC, initCim, modelSize * injCells * sizeof(double), cudaMemcpyHostToDevice);

cudaMemcpy(dev_W, W, modelSize * sizeof(double), cudaMemcpyHostToDevice);
cudaMemcpy(dev_immobilePhi, immobilePhi, modelSize * sizeof(double), cudaMemcpyHostToDevice);
cudaMemcpy(dev_mobilePhi, mobilePhi, modelSize * sizeof(double), cudaMemcpyHostToDevice);

dim3 gridDim = dim3((modelSize-2)/(TileSize-2), injCells);

for (int i = 0; i < simulations; i++) {
        AggregateConcentration<<<modelSize, 1024>>>(
                dev_immobileC, dev_mobileC, modelSize, injCells, dev_totalImmobileC, dev_totalMobileC);

        dispTerm = dt/(dx*dx)*dispCoef[i];

        RunArbitrarySimulation<<<gridDim, TileSize>>>(
                dev_immobileC, dev_mobileC,
                dev_totalImmobileC, dev_totalMobileC,
                dt, dev_W, advTerm, dispTerm, diffTerm,
                dev_immobilePhi, dev_mobilePhi,
                dev_targetImmobileC, dev_targetMobileC);

        temp = dev_targetImmobileC;
        dev_targetImmobileC = dev_immobileC;
        dev_immobileC = temp;

        temp = dev_targetMobileC;
        dev_targetMobileC = dev_mobileC;
        dev_mobileC = temp;
}

ConcentrationToDisplacement<<<dispLength, 1>>>(
        dev_immobileC + injCells, dev_mobileC + injCells,
        dev_immobilePhi + 1, dev_mobilePhi + 1, modelSize - 2, injCells, start - 1, dx, avgDisp, dev_disp);

cudaDeviceSynchronize();
```

```
	cudaMemcpy(disp, dev_disp, 2*dispLength*sizeof(double), cudaMemcpyDeviceToHost);

	MTensor dispTensor;

	int dim[2];
	dim[0] = dispLength;
	dim[1] = 2;
	libData->MTensor_new(MType_Real, 2, dim, &dispTensor);

	for (int i = 0; i < dispLength; i++) {
		dim[0] = i + 1;
		dim[1] = 1;
		libData->MTensor_setReal(dispTensor, dim, disp[Idx(i, 0, 2)]);
		dim[1] = 2;
		libData->MTensor_setReal(dispTensor, dim, disp[Idx(i, 1, 2)]);
	}

	MArgument_setMTensor(Res, dispTensor);

	cudaFree(dev_immobileC);
	cudaFree(dev_mobileC);
	cudaFree(dev_targetImmobileC);
	cudaFree(dev_targetMobileC);
	cudaFree(dev_immobilePhi);
	cudaFree(dev_mobilePhi);
	cudaFree(dev_W);
	cudaFree(dev_totalImmobileC);
	cudaFree(dev_totalMobileC);
	cudaFree(dev_disp);

	free(disp);

	return LIBRARY_NO_ERROR;
}
```